ADVANCED THEORY AND SIMULATIONS
www.advtheorysimul.com

Exploring Phase Stability and Properties of I-II$_2$-III-VI$_4$ Quaternary Chalcogenides

*Wencong Shi, Artem R. Khabibullin, and Lilia M. Woods**

A recently discovered class of quaternary chalcogenides with the I-II$_2$-III-VI$_4$ (I = Cu, Ag; II = Zn, Cd; III = Al, Ga, In; VI = S, Se, Te) chemical formula is considered using electronic structure calculations. Through cross-cation substitution and maintaining the octet rule, these materials can be obtained from the simpler II-VI zinc blende systems giving five possible structural phases; stannite, kesterite, primitive mixed CuAu, wurtzite-stannite, and wurtzite-kesterite. Here, 36 possible chemical compositions are calculated within these phases and the most stable structure is found for each material. By analyzing the lattice parameters, energy band structures, and other characteristics, different property trends of this new class of materials are presented. The electronic properties show that these materials can exhibit semiconductor to semimetal behavior depending on the phase and chemical compositions. Comparisons with other materials from the related I$_2$-II-IV-VI$_4$ systems, which are widely explored, allow for further fundamental knowledge of chalcogenide systems to be built and for the exploration of their suitability for practical applications.

1. Introduction

Multicomponent chalcogenide materials are advantageous for many applications in optoelectronics, magnetism, and transport. The diversity of such chalcogenide compositions and their flexibility of spatial arrangements are especially attractive for property modifications to answer the needs for different scientific and industrial applications. Many such systems can be derived from simpler structures by cross-cation substitution.[1] Specifically, starting with a binary II-VI zinc-blend or wurtzite system one can obtain ternary I-III-VI$_2$ or quaternary I$_2$-II-IV-VI$_4$ materials (I = Cu, Ag; II = Cd, Zn, Ta, Co, Fe, V; III = In, Ga, Al, Tl; VI = S, Se, Te).[2–5] In addition to this variety of chemical compositions, doping on different sites is also possible. As a result, one can achieve a wide range of property tuning, which has made chalcogenides and their derivatives attractive from the point of view of fundamental science and applications.[6–9] Additional motivation to further explore chalcogenides is that many of their constituents are earth-abundant and environmentally friendly,[4] which can potentially result in cost effective and ecologically clean devices.

Several representatives of the I$_2$-II-IV-VI$_4$ class of materials have emerged as good candidates for photovoltaics and solar-cell components.[10,11] The attractive properties are the tunable bandgap in the 1.0–1.5 eV range and improved device performance.[12–14] Some I$_2$-II-IV-VI$_4$ systems have also been shown to be applicable for water redox reactions.[15] Several recent reports have shown that many quaternary chalcogenides can also be good thermoelectrics.[16–20] Even though traditional thermoelectric materials are narrow band semiconductors, the inherently low thermal conductivity and tunable bandgap are key properties toward including quaternary chalcogenides in the library of thermoelectric materials.

Following the cation cross-substitution method, a rather new class of quaternary chalcogenides with the chemical formula I-II$_2$-III-VI$_4$ can also be obtained from the ternary I-III-VI$_2$. This can be achieved by obeying the octet rule and by replacing one group of I atoms and one group of III atoms in the ternary material with two groups of II atoms. Unlike the related I$_2$-II-IV-VI$_4$ chalcogenides, the I-II$_2$-III-VI$_4$ quaternary chalcogenides have been practically unexplored. A limited number of recent reports have focused primarily on synthesis and characterization. For example, it has been shown that CuTa$_2$InTe$_4$, CuZn$_2$InTe$_4$, CuCd$_2$InTe$_4$, and AgZn$_2$InTe$_4$ can synthesize in tetragonal stannite (ST) or modified cubic lattice structures and they can also have relatively low thermal conductivity.[15,21–23] Electronic structure calculations have shown that the orthorhombic wurtzite-stannite (WST) structure is possible for AgCd$_2$GaS$_4$ and AuCd$_2$GaSe$_4$, whose bandgaps are found to be ≈2.15 eV.[14] This unexplored class of quaternary chalcogenides can accommodate a large number of different elements at various lattice sites that will allow for relatively complex electronic, phonon, and structural properties determination. The tetrahedrally bonded units, which are some of the key components for low thermal conductivity in I$_2$-II-IV-VI$_4$ materials, are also expected to result in a similar property for the I-II$_2$-III-VI$_4$ materials. This is corroborated by the recent results for CuCd$_2$InTe$_4$ showing a decreasing thermal conductivity, k, with temperature, with $k \approx 1$ W m^{-1} K^{-1} at room temperature.[22,24]

W. Shi, Prof. L. M. Woods
Department of Physics
University of South Florida
Tampa, FL 33620, USA
E-mail: lmwoods@usf.edu
Dr. A. R. Khabibullin
Center for Computational Materials Science
Washington, DC 20375, USA

The ORCID identification number(s) for the author(s) of this article can be found under https://doi.org/10.1002/adts.202000041

DOI: 10.1002/adts.202000041

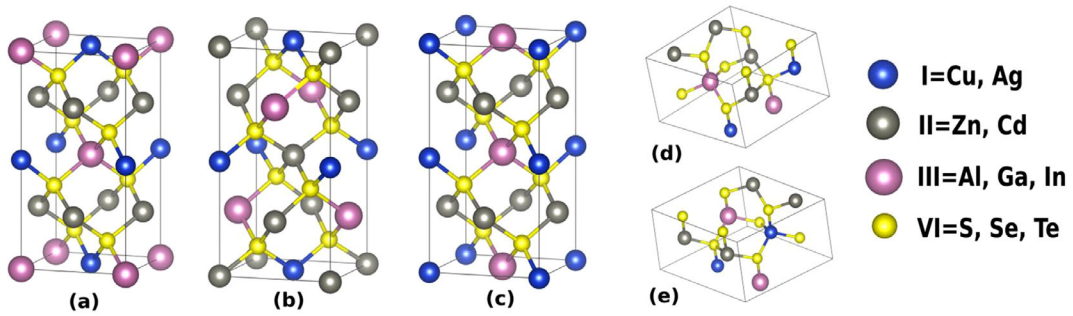

Figure 1. Crystal structures for the different phases of the quaternary I-II_2-III-VI_4 chalcogenides: a) stannite (ST), b) kesterite (KS), c) primitive mixed CuAu PMCA, d) wurtzite-kesterite (WKS), and e) wurtzite-stannite (WST). The simulated chemical compositions within each structural phase are also given in Table 1.

Table 1. All 36 Cu and Ag-based quaternary compositions investigated in the present work.

No.	Composition	No.	Composition	No.	Composition	No.	Composition	No.	Composition	No.	Composition
1	$CuZn_2InS_4$	7	$CuZn_2GaS_4$	13	$CuCd_2AlS_4$	19	$AgZn_2InS_4$	25	$AgZn_2GaS_4$	31	$AgCd_2AlS_4$
2	$CuZn_2InSe_4$	8	$CuZn_2GaSe_4$	14	$CuCd_2AlSe_4$	20	$AgZn_2InSe_4$	26	$AgZn_2GaSe_4$	32	$AgCd_2AlSe_4$
3	$CuZn_2InTe_4$	9	$CuZn_2GaTe_4$	15	$CuCd_2AlTe_4$	21	$AgZn_2InTe_4$	27	$AgZn_2GaTe_4$	33	$AgCd_2AlTe_4$
4	$CuZn_2AlS_4$	10	$CuCd_2InS_4$	16	$CuCd_2GaS_4$	22	$AgZn_2AlS_4$	28	$AgCd_2InS_4$	34	$AgCd_2GaS_4$
5	$CuZn_2AlSe_4$	11	$CuCd_2InSe_4$	17	$CuCd_2GaSe_4$	23	$AgZn_2AlSe_4$	29	$AgCd_2InSe_4$	35	$AgCd_2GaSe_4$
6	$CuZn_2AlTe_4$	12	$CuCd_2InTe_4$	18	$CuCd_2GaTe_4$	24	$AgZn_2AlTe_4$	30	$AgCd_2InTe_4$	36	$AgCd_2GaTe_4$

In this paper, we present exploratory high-throughput ab initio simulations based on density functional theory (DFT) for I-II_2-III-VI_4 quaternary chalcogenides, where I = Cu, Ag; II = Zn, Cd; III = Al, Ga, In; VI = S, Se, Te. This is a rather unexplored class of systems and we find that several phases, such as kesterite (KS), ST, wurtzite-kesterite (WKS), WST, and primitive mixed CuAu (PMCA), can be accommodated by the I-II_2-III-VI_4 chalcogenides. Importantly, these structural phases can be viewed as cation atom rearrangements starting from the chalcopyrite structure. Within DFT, we investigate the structural and energetic stability within each phase as well as the underlying electronic structure. Our systematic calculations enable us to build fundamental knowledge of this new class of quaternary chalcogenides and compare it with the related and much more explored I_2-II-IV-VI_4 systems.

2. Results and Discussion

2.1. Crystal Structures

The I-II_2-III-VI_4 family of materials is a derivative of the I-III-VI_2 ternary compounds, which typically synthesize in the chalcopyrite structure (space group $I\bar{4}2d$). The chalcopyrite structure is characterized by the chalcogen atoms group being surrounded by the I and III atomic groups, which is a manifestation of the octet rule. Substituting one group of I atoms and one group of III atoms with two groups of II atoms results in the quaternary I-II_2-III-VI_4 systems, in which further cation rearrangement results in several possible phases. These include the KS (space group $I\bar{4}$), ST (space group $I\bar{4}2m$), WKS (space group Pc), WST (space group $Pmn2_1$), and PMCA (space group $P\bar{4}2m$). **Figure 1** shows the respective lattice structures for these phases and **Table 1** contains the list of all chemical compositions investigated here. We note that similar lattice structures have been observed in the related I_2-II-IV-VI_4 systems, which are also derived from the ternary chalcopyrites.[13,25] As the atoms within each group are changed, a variety of chemical compositions are obtained. In Table 1, we summarize the considered compounds within each structural phase as given in Figure 1a–e.

From the geometry of each phase, it is evident that the KS and ST structures have tetragonal symmetry. Additionally, the ST phase can be characterized as having alternating layers composed of II–VI atoms and I-III atoms along the vertical direction, as shown in Figure 1a. On the other hand, the PMCA structure can be viewed as two repeating units stacked vertically, where each unit is derived from the CuAu binary zinc-blend by atomic cross-substitution.[2] The wurtzite phases are hexagonal crystal structures whose prototype typically is given as the one for ZnS.[26] The wurtzite-stannite and wurtzite-kesterite structures are derived from the wurtzite lattice based upon the valence octet rule.[3] One notes that in addition to the stability originating from the inherent structural symmetry, the different cations and chalcogens will also be important. Their sizes will affect the lattice parameters of the considered materials, which further influence the structural and energetic stability of these systems.

2.2. Computation Methods

In order to understand the basic properties of the chemical compositions within each phase (Figure 1) we use density functional theory as implemented in the Vienna ab initio simulation package (VASP).[27,28] By performing high-throughput

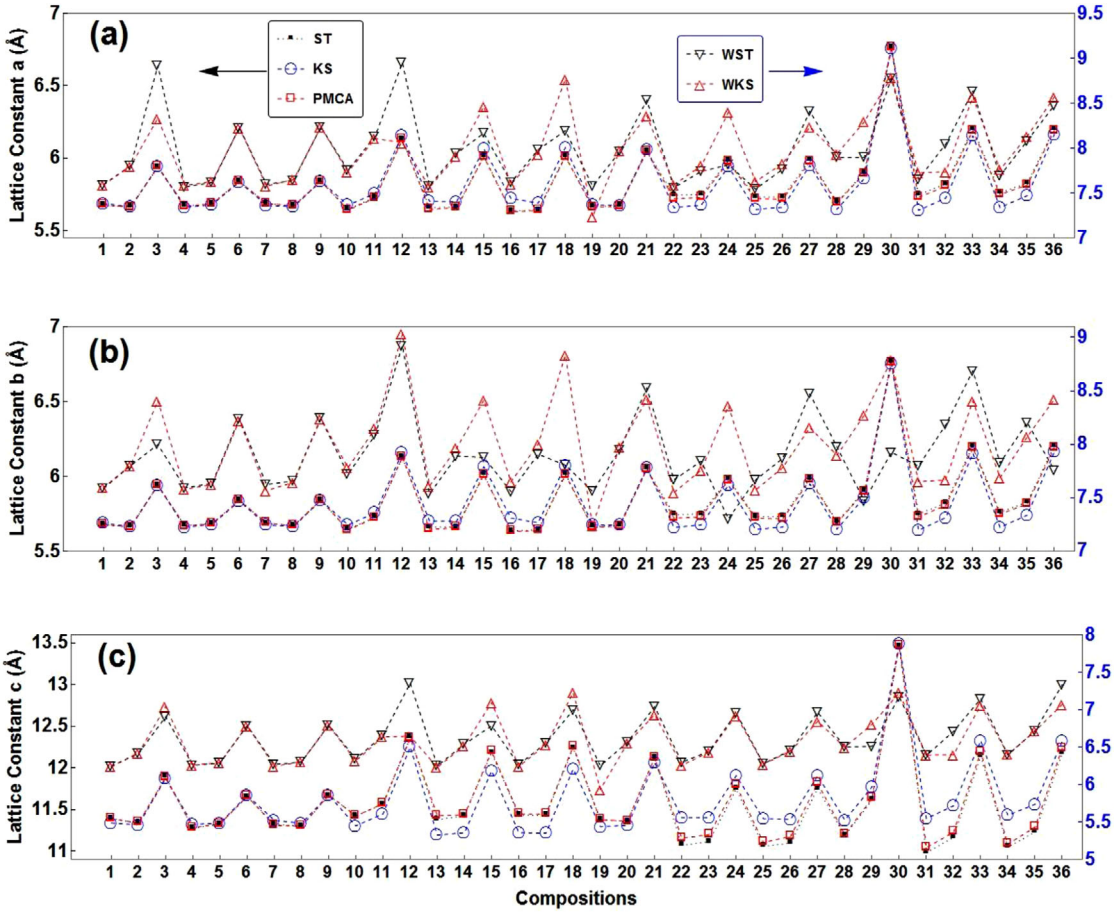

Figure 2. Structural parameters in Å for the considered I-II_2-III-VI_4 compounds: a) lattice constant *a*, b) lattice constant *b*, and c) lattice constant *c*. The left *y*−axis corresponds to Cu-based materials (scale in black) and the right *y*−axis corresponds to Ag-based materials (scale in blue). The composition numbering can be found in Table 1.

calculations the structural stability, lattice parameters, and electronic properties are studied of the I-II_2-III-VI_4 family of materials. The computation procedure utilized in VASP is based on a projector-augmented wave method which adopts a plane-wave basis and periodic boundary conditions. For the exchange-correlation energy, a generalized gradient approximation (GGA) with Perdew–Burke–Ernzerhof (PBE) functional is applied.[29] In the relaxation process, convergence criteria for total energy are chosen as 10^{-5} eV and total force 10^{-4} eV Å^{-1}, respectively. The energy cutoff for each quaternary structure is chosen as the maximum default cutoff energy of the four atoms multiplied by 1.3, as per VASP guidelines to guarantee the complete enough basis set. The *k*-point mesh is chosen to be 12 × 12 × 12 and the tetrahedron integration method with Blöchl corrections are used in GGA-PBE.

2.3. Phase Stability

Using the described ab initio methods each chemical composition is simulated for the five structural phases, as shown in Figure 1 and Table 1. All materials are found to be stable after relaxation and results for the three lattice constants are given in **Figure 2**. One finds that *a, b,* and *c* exhibit an oscillatory-like behavior with respect to changing the chalcogen atom. This is easily understood since the largest Te atom promotes larger lattice constants, while the smallest S atom results in the smaller *a, b,* and *c* for each phase, as seen in Figure 2. The overall smaller *a, b, c* constants for compositions with $N = [1, 18]$ as compared to those for the rest of the compounds are explained with the size of the Cu and Ag atoms (the Cu atom is smaller than the Ag atom).

From the simulations it is determined that for the ST, KS, and PMCA, $a = b \approx \frac{1}{2}c$, while for the WKS and WST $a \approx b > c$. Another important trend found in Figure 2 is that kesterites, stannites, and PMCA systems have smaller lattice parameters, while practically all WKS and WST phases have larger lattice parameters. In some cases, however, the differences within KS, ST, and PMCA and WKS, WST for a given composition are rather small, for example, for $CuZn_2GaTe_4$ *a*=*b*=5.843 Å, *c*=11.665 Å (ST), *a*=*b*=5.842 Å, *c*=11.674 Å (KS), *a*=*b*=5.841 Å, *c*=11.676 Å (PMCA), *a*=8.236 Å, *b*=8.243 Å, *c*=6.795 Å (WST), *a*=8.235 Å, *b*=8.239 Å, *c*=6.788 Å (WKS). For other compositions, these lattice constants have larger variation, for example, for $AgZn_2GaSe_4$ *a*=*b*=5.733 Å, *c*=11.095 Å (ST), *a*=*b*=5.662 Å, *c*=11.381 Å (KS), *a*=*b*=5.717 Å, *c*=11.1758 Å (PMCA), and *a*=7.765 Å, *b*=7.869 Å, *c*=6.455 Å (WST), *a*=7.831 Å, *b*=7.783 Å, *c*=6.446 Å (WKS). It is

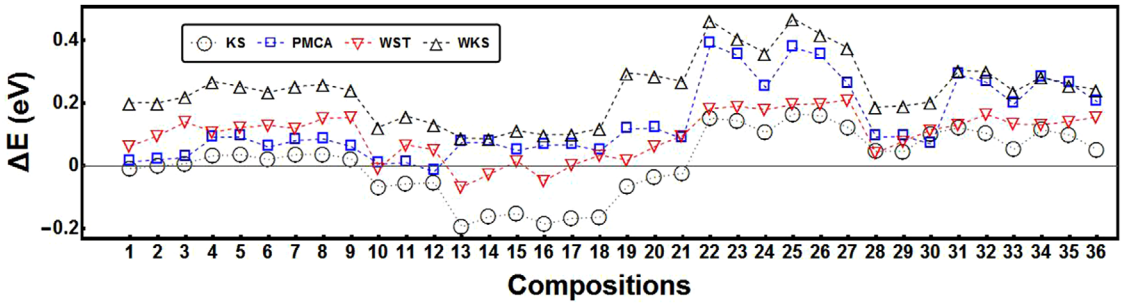

Figure 3. The total energy differences $\Delta E = E_{Ph} - E_{ST}$ for Ph = KS, PMCA, WST, WKS are shown for the considered materials. The composition numbering can be found in Table 1.

Table 2. Formation energy per atom $\bar{E}_f$ (in eV) for the considered compounds. The compositional numbering is the same as in Table 1. The most stable phase is denoted in brackets next to each material.

No.	$\bar{E}_f$	No.	$\bar{E}_f$	No.	$\bar{E}_f$	No.	$\bar{E}_f$	No.	$\bar{E}_f$	No.	$\bar{E}_f$
1	−0.644 (KS)	7	−0.690 (ST)	13	−0.717 (KS)	19	−0.770 (KS)	25	−0.816 (ST)	31	−0.843 (ST)
2	−0.571 (KS)	8	−0.591 (ST)	14	−0.623 (KS)	20	−0.697 (KS)	26	−0.717 (ST)	32	−0.749 (ST)
3	−0.370 (ST)	9	−0.372 (ST)	15	−0.396 (KS)	21	−0.496 (KS)	27	−0.498 (ST)	33	−0.522 (ST)
4	−0.809 (ST)	10	−0.559 (KS)	16	−0.596 (KS)	22	−0.935 (ST)	28	−0.685 (ST)	34	−0.722 (ST)
5	−0.669 (ST)	11	−0.531 (KS)	17	−0.543 (KS)	23	−0.795 (ST)	29	−0.657 (ST)	35	−0.669 (ST)
6	−0.405 (ST)	12	−0.365 (KS)	18	−0.361 (KS)	24	−0.531 (ST)	30	−0.491 (ST)	36	−0.487 (ST)

interesting to note that the lattice parameters for the KS, ST, and PMCA phases for many chemical compositions can be quite similar. This is expected given the related symmetries of these phases in which the positions for the chalcogen atoms is the same and the cation atoms (most have close in value ionic radii) are rearranged. Such comparison can be made for the WST and WKS phases.

We further investigate the energetic stability of the considered family of materials by comparing the relative total energy across different phases. For this purpose, by choosing ST as a baseline for comparison the differences $\Delta E_{Ph-ST} = E_{Ph} - E_{ST}$ for each Ph = KS, PMCA, WKS, WST are calculated and plotted in **Figure 3**. One finds that for the Cu-based structures, the ST phase is the most energetically stable one for the $N = 2$–9 compositions (Table 1), while the KS phase is preferred by $N = 1$, 10–18 compounds. Only three Ag-based systems ($N = 19$–21) have KS as the most stable one, while for the rest the ST phase is the one with lowest total energy. For all studied materials the WKS is the least energetically stable state (it has the highest total energy) followed by the WST. These results correlate with the structural trends found in Figure 2, such that most energetically stable systems have the smallest lattice parameters, while the least energetically stable systems have the largest lattice structures.

The average formation energies for the most stable phases for the considered compositions are also calculated using the expressions $\bar{E}_f = \frac{1}{n}(E_T - \sum_{i=1}^{N} E_i)$, where E_T is the total energy of the compound and E_i is the energy of the constituent atoms[30] (n is the number of atoms in the unit cell). The results are gathered in **Table 2**, where the most stable phase for each composition is denoted in brackets. One finds that $\bar{E}_f$ follows an oscillatory-like pattern consistent with variation in atomic radii magnitudes—smallest for the S atom and larges for the Te atom. Specifically, the largest $|\bar{E}_f|$ is found for S-based chalcogenides, while the smallest $|\bar{E}_f|$ is calculated for the Te-based systems. This trend correlates with the structural data displayed in Figure 2.

2.4. Electronic Structures

We further investigate the electronic structure of the I-II$_2$-III-VI$_4$ chalcogenides within each structural phase from Figure 1. After obtaining the energy band structure and density of states (DOS) for the relaxed systems, the energy bandgaps for all materials are calculated and given in **Figure 4**. The results show that this family of materials can exhibit diverse type of transport that is characteristic for semimetals and semiconductors. For example, for $CuZn_2InSe_4$ $E_g = 0.156$ eV (KS), for $CuZn_2AlS_4$ $E_g = 1.579$ eV (ST), $AgZn_2GaSe_4$ $E_g = 0.612$ eV (ST), $AgCd_2GaSe_4$ $E_g = 0.9072$ eV (ST). Also, while the bandgap values in Figure 4 are of similar order for different structural phases of the each compound, the variations in E_g within the Ag-based compositions are greater than Cu-based compositions as can be seen from the higher peaks for compositions $N = 19$–36. Additionally, the largest E_g is found for the most energetically favorable structure within the possible phases for a given material in most cases. Similar to Figure 2, an oscillatory-like trend as a function of composition is obtained for the energy gap behavior for the Cu and Ag-based materials. However, the oscillatory maxima in E_g are found for systems with S chalcogens, while the E_g oscillatory minima are for systems with Se chalcogens for almost all phases, which agrees with basic chemistry principles for S- and Se-based compounds.

To further study the electronic structure trends, the energy band structures for several of the considered materials are shown

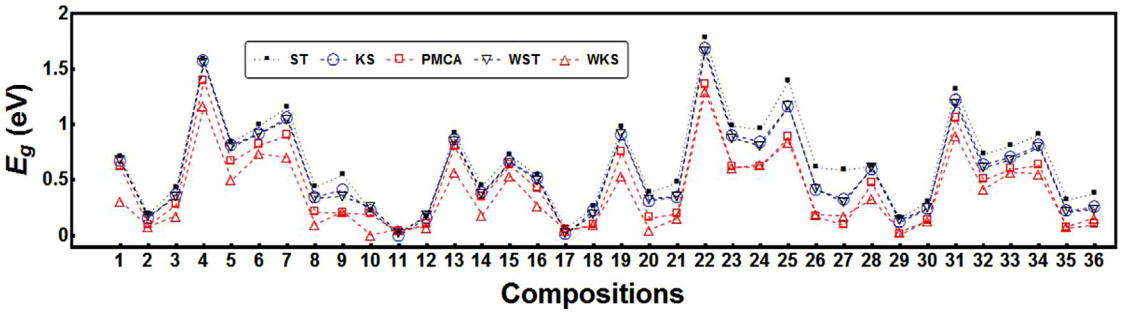

Figure 4. Bandgap energies for all considered compounds. The composition numbering can be found in Table 1.

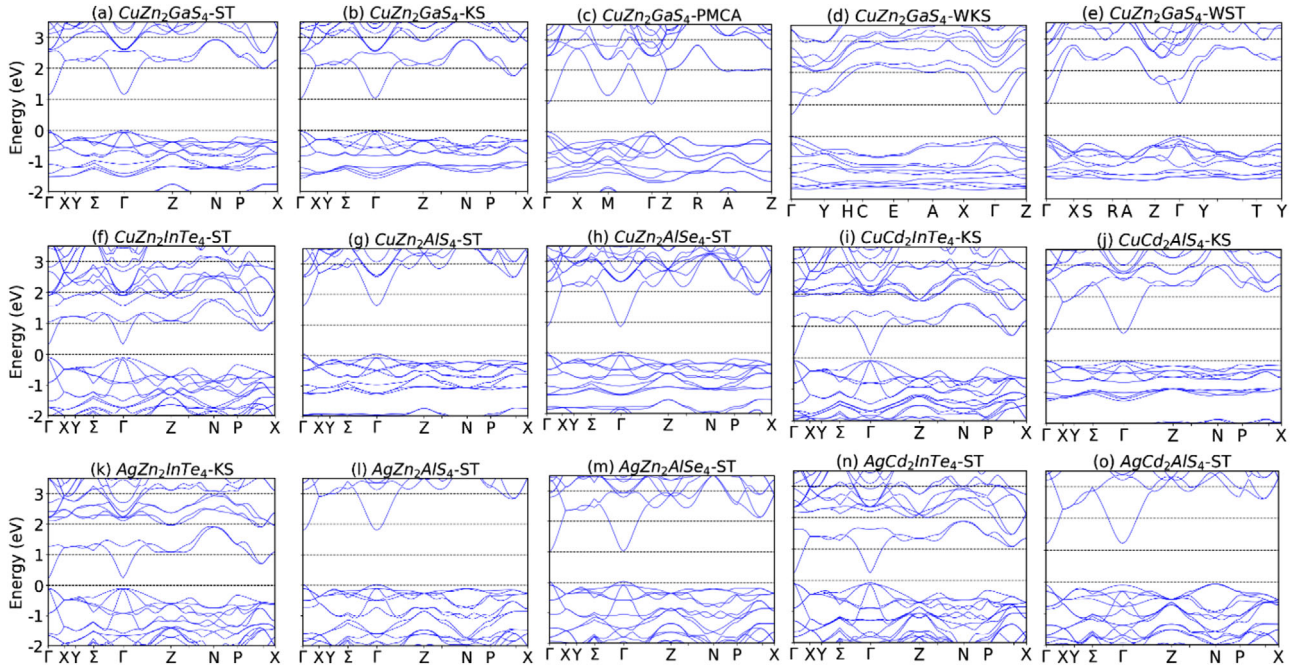

Figure 5. Band structures of a–e) five phases for the composition $CuZn_2GaS_4$; f–j) the most stable phase for the Cu-based structures with $N = 3$, 4, 5, 12, 13; and k–o) the most stable phase for the Ag-based structures with $N = 21$, 22, 23, 30, 31, as denoted in Table 1.

in **Figure 5**. The energy bands of the $CuZn_2GaS_4$ compound in its five phases are displayed in Figure 5a–e, while the most energetically favorable phase of several corresponding Cu- and Ag-based materials are displayed in Figure 5f–o. In most cases, all materials are n-type semiconductors with direct energy gaps at the Γ-point. The Fermi level lies on top of relatively flat highest valence bands. The lowest conduction band has a distinct minimum at the Γ-point. For many of the compounds with an In cation, the gap reduces significantly and in some situations the material can exhibit a semimetallic behavior as is the case for $CuCd_2InTe_4$ (Figure 5i).

In **Figure 6** results for the total and orbitally projected DOS are shown for some of the materials, which helps us to understand the makeup of the states especially around the Fermi level. There is a strong hybridization between the Cu, Cd and chalcogenide atoms in $CuCd_2InTe_4$ (Figure 6a) and $CuCd_2AlS_4$ (Figure 6b) in the valence region near E_F, though Cd atoms contribute less than the Cu atoms; similar hybridization between the corresponding cation and chalcogenide atoms occurs right below the Fermi level in $AgZn_2AlSe_4$ (Figure 6c), $AgCd_2InTe_4$ (Figure 6d), and $AgCd_2AlS_4$ (Figure 6e). In the conduction region at the top of the gap, we observe hybridization between Cd, In and Cd, Al although DOS is rather small compared to the DOS in the valence region. In some of the materials, more than one gaps are observed below E_F. For example, in $CuCd_2InS_4$ (Figure 6b) secondary gaps below Fermi level are found to be 0.076 eV in the (−0.883 eV, −0.726 eV) range and 0.471 eV in the (−1.825 eV, −1.354 eV) range. Similarly, the states around those gaps are predominantly from hybridized Cd, Zn and chalcogenide atoms orbitals. We note that the orbital DOS composition (especially the strong I–VI atomic hybridization) around E_F is rather similar to the one of the related family of I-II_2-III-VI_4 compounds[3] in their corresponding KS and ST phases.

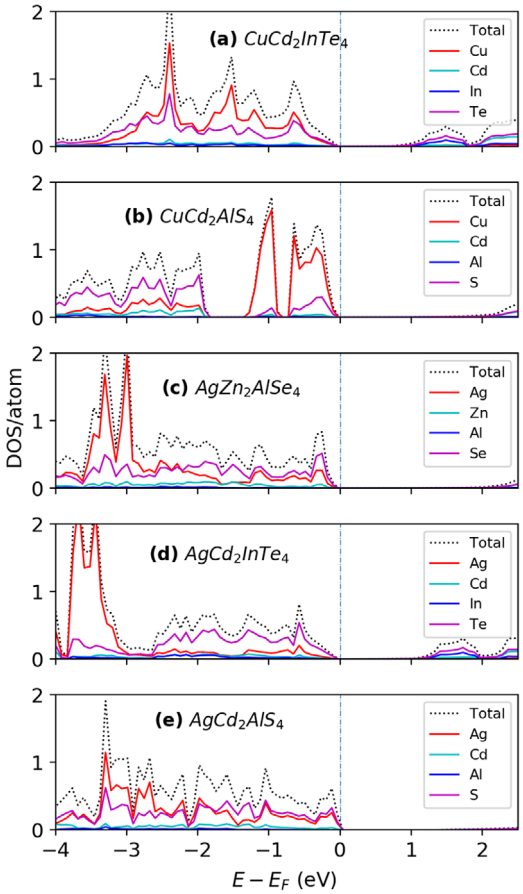

Figure 6. Total and atomically projected DOS per atom plots for a) $CuCd_2InTe_4$, b) $CuCd_2AlS_4$, c) $AgZn_2AlSe_4$, d) $AgCd_2InTe_4$, and e) $AgCd_2AlS_4$.

3. Conclusion

In this paper, DFT calculations are performed for a large class of I-II_2-III-VI_4 quaternary materials, using GGA approximation implemented in VASP, the energies as function of compositions for the given structures are studied and compared, the lattice constants are obtained for the fully relaxed structures. The bandgaps for the structures are obtained which can provide convenient comparisons for experimental measurements. Some typical band structures for a few selected structures with wide, narrow and near-zero bandgaps are shown also. The large diversity of E_g values shows that different cation and chalcogen atomic compositions can be used to achieve semiconductors with direct gaps of various magnitudes at the Γ point. These electronic properties, the structural and compositional similarities of the I-II_2-III-VI_4 class to the much more explored I_2-II-IV-VI_4 chalcogenides, and recent transport experimental studies showing encouraging low thermal conductivity[16,17] suggest that I-II_2-III-VI_4 chalcogenides may also be beneficial for thermoelectric and photovoltaic applications. Our comprehensive investigation sets the foundation for further experimental and computational investigations of this unexplored class of materials in terms of utilizing doping, external fields, temperature among other factors to find effective ways for property modifications. Such studies are necessary in order to understand the suitability of these systems for applications, such as thermoelectricity and photovoltaics.

Acknowledgements

L.M.W. acknowledges support from the US National Science Foundation (NSF) under Grant No. DMR-1748188. A.R.K acknowledges support from the National Research Council fellowship at the U.S. Naval Research Laboratory. We also would like to thank Dr. S. Erwin for assistance with this paper.

Conflict of Interest

The authors declare no conflict of interest.

Keywords

ab initio calculations, electronic properties, quaternary chalcogenides, thermoelectricity

Received: March 4, 2020
Revised: April 11, 2020
Published online: May 25, 2020

[1] C. H. L. Goodman, *J. Phys. Chem. Solids* **1958**, *6*, 305.
[2] S. Chen, X. G. Gong, A. Walsh, S.-H. Wei, *Phys. Rev. B* **2009**, *79*, 165211.
[3] S. Chen, A. Walsh, Y. Luo, J.-H. Yang, X. G. Gong, S.-H. Wei, *Phys. Rev. B* **2010**, *82*, 195203.
[4] J. Kim, L. Larina, S. Y. Chung, D. Shin, B. Shin, *J. Mater. Res.* **2018**, *33*, 3986.
[5] L. Zhao, N. Lin; Z. Han, X. Li, H. Wang, J. Cui, *Adv. Electron. Mater.* **2019**, *5*, 1900485.
[6] C. K. Williams, T. H. Glisson, J. R., Hauser, M. A. Littlejohn, *J. Electron. Mater.* **1978**, *7*, 639.
[7] A. Pan, R. Liu, M. Sun, C.-Z. Ning, *J. Am. Chem. Soc.* **2009**, *131*, 9502.
[8] R. Freer, A. V. Powell, *J. Mater. Chem. C* **2019**, *8*, 441.
[9] D. Chen, Y. Zhao, Y. Chen, T. Lu, Y. Wang, J. Zhou, Z. Liang, *Adv. Electron. Mater.* **2016**, *2*, 1500473.
[10] D. A. R. Barkhouse, O. Gunawan, T. Gokmen, T. K. Todorov, D. B. Mitzi, *Prog. Photovoltaics* **2012**, *20*, 6.
[11] M. Ibáñez, R. Zamani, A. LaLonde, D. Cadavid, W. Li, A. Shavel, J. Arbiol, J. R. Morante, S. Gorsse, G. J. Snyder, A. Cabot, *J. Am. Chem. Soc.* **2012**, *134*, 4060.
[12] T. Jing, Y. Dai, X. Ma, W. Wei, B. Huang, *J. Phys. Chem. C* **2015**, *119*, 27900.
[13] A. Ghosh, S. Palchoudhury, R. Thangavel, Z. Zhou, N. Naghibolashrafi, K. Ramasamy, A. Gupta, *Chem. Commun.* **2016**, *52*, 264.
[14] V. L. Bekenev, V. V. Bozhko, O. V. Parasyuk, G. E. Davydyuk, L. V. Bulatetska, A. O. Fedorchuk, I. V. Kityk, O. Y. Khyzhun, *J. Electron Spectrosc. Relat. Phenom.* **2012**, *185*, 559.
[15] G. E. Delgado, A. J. Mora, P. Grima-Gallardo, S. Durán, M. Muñoz, M. Quintero, *Cryst. Res. Technol.* **2008**, *43*, 783.
[16] T. Gürel, A. Mcferrin, *Phys. Rev. B* **2011**, *84*, 205201.
[17] D. Hobbis, W. Shi, A. Popescu, K. Wei, R. E. Baumbach, H. Wang, L. M. Woods, G. S, Nolas, *Dalton Trans.* **2020**, *49*, 2273.

[18] Q. Song, P. Qiu, H. Chen, K. Zhao, D. Ren, X. Shi, L. Chen, *ACS Appl. Mater. Interfaces* **2018**, *10*, 10123.
[19] D. Hobbis, K. Wei, H. Wang, G. S. Nolas, *J. Alloys Compd.* **2018**, *743*, 543.
[20] Q. Song, P. Qiu, F. Hao, K. Zhao, T. Zhang, D. Ren, X. Shi, L. Chen, *Adv. Electron. Mater.* **2016**, *2*, 1600312.
[21] G. S. Nolas, M. S. Hassan, Y. Dong, J. Martin, *J. Solid State Chem.* **2016**, *242*, 50.
[22] D. Hobbis, K. Wei, H. Wang, G. S. Nolas, *J. Alloys Compd.* **2018**, *743*, 543.
[23] W. Shi, A. R. Khabibullin, D. Hobbis, G. S. Nolas, L. M. Woods, *J. Appl. Phys.* **2019**, *125*, 155101.
[24] G. S. Nolas, M. S. Hassan, Y. Dong, J. Martin, *J. Solid State Chem.* **2016**, *242*, 50.
[25] T. Gürel, C. Sevik, T. Çağın, *Phys. Rev. B* **2011**, *84*, 205201.
[26] H. Wonderatschek, U. Müller, *International Tables for Crystallography: Volume A1: Symmetry Relations Between Space Groups*, Springer, Dordrecht, **2008**.
[27] G. Kresse, J. Furthmüller, *Comput. Mater. Sci.* **1996**, *6*, 15.
[28] G. Kresse, J. Furthmüller, *Phys. Rev. B* **1996**, *54*, 11169.
[29] J. P. Perdew, K. Burke, M. Ernzerhof, *Phys. Rev. Lett.* **1996**, *77*, 3865.
[30] M. De Jong, W. Chen, T. Angsten, A. Jain, R. Notestine, A. Gamst, M. Sluiter, C. K. Ande, S. Van Der Zwaag, J. J. Plata, C. Toher, S. Curtarolo, G. Ceder, K. A. Persson, M. Asta, *Sci. Data* **2015**, *2*, 150009.